Hindawi Publishing Corporation
Advances in Materials Science and Engineering
Volume 2015, Article ID 249348, 6 pages
http://dx.doi.org/10.1155/2015/249348

Research Article

Synthesis, Structure, and Electrical Property of $Ce_{1-x}Sr_{1+x}Ga_3O_{7-\delta}$

Xiaohui Li, Jungu Xu, Junshu Xiaofeng, and Xiaojun Kuang

Guangxi Ministry-Province Jointly-Constructed Cultivation Base for State Key Laboratory of Processing for Non-Ferrous Metal and Featured Materials, MOE Key Laboratory of New Processing Technology for Nonferrous Metals and Materials, College of Materials Science and Engineering, Guangxi Universities Key Laboratory of Non-Ferrous Metal Oxide Electronic Functional Materials and Devices, Guilin University of Technology, Guilin 541004, China

Correspondence should be addressed to Jungu Xu; xujungu@126.com

Received 6 October 2015; Revised 14 December 2015; Accepted 14 December 2015

Academic Editor: Massimiliano Barletta

Copyright © 2015 Xiaohui Li et al. This is an open access article distributed under the Creative Commons Attribution License, which permits unrestricted use, distribution, and reproduction in any medium, provided the original work is properly cited.

$Ce_{1-x}Sr_{1+x}Ga_3O_{7-\delta}$ powders were synthesized by a solid state reaction method under reducing atmosphere. Single melilite phase was obtained for $x \leq 0.2$. X-ray diffraction pattern displays a preferred orientation on (002) peak of the $Ce_{0.9}Sr_{1.1}Ga_3O_{7-\delta}$ composition. Scanning electron microscope disclosed the nanoscale needle-like micromorphology of this material, with an average length of ~2.5 μm and a diameter of ~500 nm. Transmission electron microscopy and selected area electron diffraction reveal the single crystal nature of these individual $Ce_{0.9}Sr_{1.1}Ga_3O_{7-\delta}$ needles and build up a relationship between the preferred orientation observed in X-ray diffraction pattern and the micromorphology. The phase stability of $Ce_{1-x}Sr_{1+x}Ga_3O_{7-\delta}$ in air was studied and the electrical property was investigated by impedance spectroscopy.

1. Introduction

Oxide ion conductors with high ionic conductivity attract considerable attention because of their important applications in many fields, such as oxygen sensors, oxygen permeation membranes, and solid oxide fuel cells (SOFCs). The SOFC is a promising technology for clean energy conversion with high efficiency and fuel flexibility [1–3]. Pure oxide ion conductors with negligible electronic conduction and oxide ion conductivity exceeding 10^{-2} S/cm are required for the application as electrolyte in SOFCs. Yttria-stabilized zirconia (YSZ), the currently commercially used electrolyte in SOFCs, reaches this target at 700°C [3]. Given the drive towards lowering device-operating temperatures, there is a strong impetus and a great challenge to develop materials with enhanced ionic mobility and to understand the fundamental mechanism controlling the oxide ion motion at atomic level [4, 5].

The $LaSrGa_3O_7$-based materials are recently investigated as a promising electrolyte candidate for SOFCs [6–11]. The parent material $LaSrGa_3O_7$ adopts the $A_2B_3O_7$ (A_2 = LaSr, B = Ga) melilite structure [12], The cation ratio of La/Sr is alternating, and the corner-shared GaO_4 tetrahedral compose 5-fold tetrahedral rings. The eight-coordinate A site cations locate above/below the 5-fold ring centers, as shown in Figure 1. By varying the cationic stoichiometry, $La_{1+x}Sr_{1-x}Ga_3O_{7+0.5x}$ becomes an interstitial oxide ion conductor when excess oxygen from substitution of La^{3+} for Sr^{2+} is introduced within the structure. For example, the composition of $La_{1.54}Sr_{0.46}Ga_3O_{7.27}$ shows pure oxide ion conductivity of 0.02–0.1 S/cm over the temperature range of 600–900°C [9]. The interstitial oxygen ions are accommodated between the layers within the 5-fold channels in the average structure, and for the local structure the excess oxygen ions would transform one GaO_4 tetrahedron among the five tetrahedra defining the 5-fold ring into a bipyramidal GaO_5 polyhedron. The interstitial oxide anions are transported via a hopping mechanism among the pentagonal tunnels in the 2D Ga_3O_7 layers according to a cooperation mechanism involving the rotation and deformation of the tetrahedral framework [9] thanks to the existence of nonbridging terminal oxygen in the layered tetrahedral network.

In our previous study, La^{3+} ions in $LaSrGa_3O_7$ were shown to be completely replaced by Ce^{3+} ions and the oxidization of Ce^{3+} to Ce^{4+} in the $CeSrGa_3O_7$ may introduce

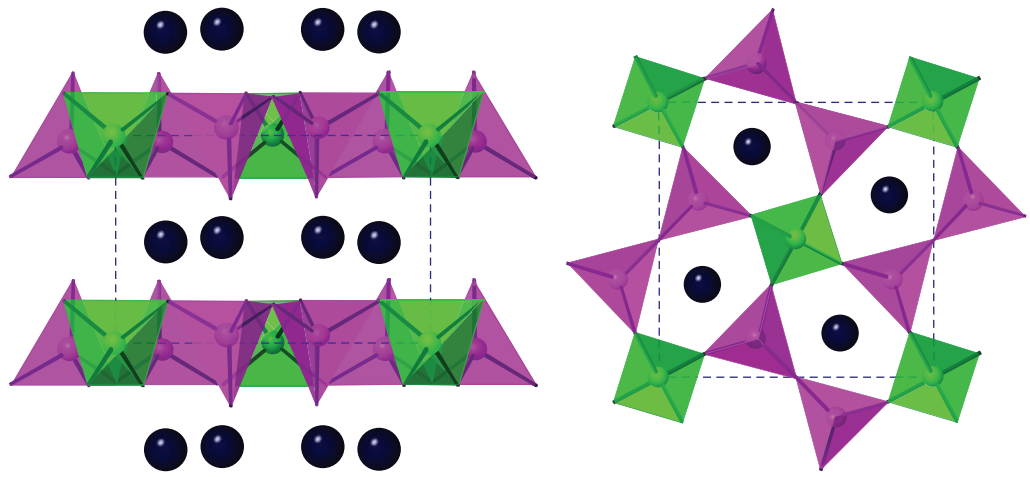

Figure 1: Melilite structure of $LaSrGa_3O_7$. (a) View along the b axis, showing the layered nature of the structure. The black spheres and polyhedra denote La/Sr atoms and GaO_4 tetrahedra, respectively. (b) View along the c axis, showing the connectivity of the Ga tetrahedral units forming distorted pentagonal tunnels. The La/Sr atoms above or below the centers of the pentagonal.

excess oxygen [13]. Such excess oxygen was shown to be immobile in great contrast with $La_{1+x}Sr_{1-x}Ga_3O_{7+0.5x}$ case. Analysis of the neutron powder diffraction (NPD) data of $CeSrGa_3O_{7.39}$ revealed a new way for accommodating the oxygen interstitials in $CeSrGa_3O_{7.39}$ with the melilite structure via being located at the framework oxygen level and being incorporated into the coordination environment of a 4-linked GaO_4 tetrahedron, leading to a distorted GaO_5 trigonal bipyramid. The 4-linked GaO_4 has constrained rotation and deformation because of the absence of nonbridging terminal oxygen; the smaller Ce^{4+} in the A cationic layer placed strong bonding with oxygen interstitials; both factors constrain the mobility of oxygen interstitials $CeSrGa_3O_{7+\delta}$ [13].

In $CeSrGa_3O_{7+\delta}$, extending Ce/Sr ratio toward Ce-rich side was found to be difficult in our previous study [13]. Here, in this work, the effort was put into preparation, microstructure, and electrical properties of the Sr-rich composition $Ce_{1-x}Sr_{1+x}Ga_3O_{7-\delta}$. The XRD pattern of $Ce_{0.9}Sr_{1.1}Ga_3O_{7-\delta}$ has shown a preferred orientation along (002) plane, which coincides with the nanoscale stick-like micromorphology and growth direction along [001], as revealed by SEM and HRTEM. This demonstrated a rare example of nanomaterials prepared by solid state reaction method.

2. Experimental

The starting materials of CeO_2 (99.99%), $SrCO_3$ (99.0 + %), and Ga_2O_3 (99.99%) were used to prepare the polycrystalline $Ce_{1-x}Sr_{1+x}Ga_3O_{7-\delta}$ samples. For composition $x = 0.1$, the mixture of starting materials (with 6 mol% excess of Ga_2O_3 to compensate for the Ga_2O_3 volatilization during the high temperature firing) was first sintered at 1200°C for 12 h in air and then 1300°C for 12 h in CO-reducing atmosphere produced by the incomplete combustion of carbon powder, and then the grinded powders were fired at 1350°C for 12 h CO-reducing atmosphere. Material $x = 0.2$ was prepared by reaction, the stoichiometry starting materials (with 6 mol% excess of Ga_2O_3) at 1200°C for 12 h in air, and then fired at 1305°C for 12 h in CO-reducing atmosphere. Ceramic pellet samples were made via uniaxially pressing with 320 MPa pressure after being calcined at 1200°C for 12 h in air and then fired under the same condition with powder samples. Two ceramic pellets were prepared for each composition: one was used for XRD characterization after being ground into powder, and the other was used for alternating current (AC) impedance spectroscopy (IS) measurements.

The X-ray diffraction (XRD) was performed on a D8 ADVANCE powder diffractometer with Cu Kα radiation at room temperature. Rietveld refinements were performed using Topas Academic software [14]. A JEM-2010HR transmission electron microscope (200 kV) instrument was used for the transmission electron microscopy (TEM) and selected area electron diffraction (SAED) study. Scanning electron microscope (SEM) measurement was performed on a FEI Quanta 400 Thermal FE Environment scanning electron microscope. Alternating current (AC) impedance spectroscopy (IS) measurements under air were carried out by using a Solartron 1260A impedance/gain-phase analyzer over the 10^{-1} to 10^7 Hz range. Prior to the IS measurement, the pellet was coated with gold paste (depending on the stability temperature of the pellets), which were fired at 500°C for 30 min to burn out the organic components to form electrodes.

3. Results and Discussion

3.1. Phase Relationship. For the $Ce_{1-x}Sr_{1+x}Ga_3O_{7-\delta}$ nominal compositions, single melilite phase products can be obtained for $x \leq 0.2$ only, as shown in Figure 2. The XRD patterns show similar results for the powder samples and pellet samples. For $x > 0.2$, we tried many different calcining temperatures

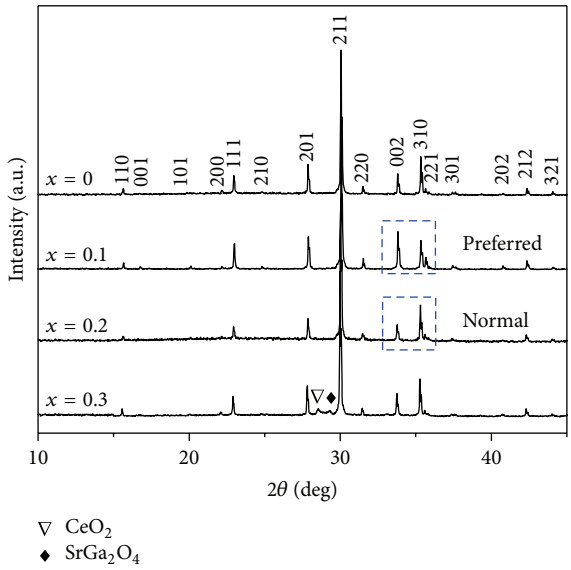

FIGURE 2: XRD patterns of the as-made $Ce_{1-x}Sr_{1+x}Ga_3O_{7-\delta}$ ($x = 0.1$, 0.2, and 0.3) in this work, together with the XRD pattern of $x = 0$ as had been reported in our previous work [13] for comparison.

and they all failed to get pure phase product, with impurity phases CeO_2 and $SrGa_2O_4$ being detected. The XRD pattern of sample $x = 0.3$ was prepared by firing the powders at 1300°C. This narrow solid solution region is similar to that for $La_{1-x}Sr_{1+x}Ga_3O_{7-0.5x}$ as reported in our recently published work [15]. For $La_{1-x}Sr_{1+x}Ga_3O_{7-0.5x}$, the narrow solid solution region was attributed to the high defect formation energy of Sr^{2+} substitution for La^{3+} compared to the smaller defect formation energy of La^{3+} substitution for Sr^{2+} [15].

The cell parameters of compositions $x = 0.2$ and $x = 0.1$, derived from Rietveld refinements based on the structure of $LaSrGa_3O_7$ [12], are $a = 8.0476(2)$ Å, $c = 5.3152(2)$ Å, and $a = 8.0443(2)$ Å and $c = 5.3095(1)$ Å, respectively. The cell parameters of the as-made $CeSrGa_3O_{7+\delta}$ [13] are $a = 8.0391(1)$ Å, $c = 5.3052(1)$ Å. We can see, the lattice parameters increase with the Sr/Ce ratio in the materials, due to the Sr^{2+} (ionic radius 1.26 Å in 8-coordinate cations) substitution for the smaller Ce^{3+}/Ce^{4+} (1.14/0.97 Å) [16]. As can be seen in Figure 2, the XRD pattern of composition $x = 0.1$ displays a stronger preferred orientation along (002) plane than the other compositions, indicating a special morphology of this sample. This phenomena was investigated in the following section.

3.2. Microstructure. As stated above, the XRD pattern of $Ce_{0.9}Sr_{1.1}Ga_3O_{7-\delta}$ displays a preferred orientation on the peak of (002), which may be a suggestion of special morphology for this composition. Thus, characterizations of SEM, TEM, HRTEM, and SAED measurements were subsequently performed on the powder of this composition. The SEM photos demonstrated that $Ce_{0.9}Sr_{1.1}Ga_3O_{7-\delta}$ powders have shown uniform needle-like morphology and these needles have an average length and diameter of about 2.5 μm and 500 nm, respectively, as can be appreciated in Figure 3(a). The materials of $Ce_{1-x}Sr_{1+x}Ga_3O_{7-\delta}$ without preferred orientation in the XRD patterns display morphology with randomly orientated grains, as shown for the $CeSrGa_3O_{7+\delta}$ material as an example in Figure 3(b).

Figure 4(a) is the representative low-magnification TEM image of a single $Ce_{0.9}Sr_{1.1}Ga_3O_{7-\delta}$ needle. The length and diameter of this needle in the TEM image are consistent with the SEM observations. The HRTEM image in Figure 4(b) was taken from the area marked by an open circle of the needle in Figure 4(a), and the one-dimensional lattice fringes appeared. The lattice spacing was found to be approximately 8.04 Å, which matched well (100) or (010) plane of the tetragonal $Ce_{0.9}Sr_{1.1}Ga_3O_{7-\delta}$ material, indicating the crystal growth direction along [100] or [010], respectively, parallel to the needle axis. This therefore facilitated preserving the plane parallel to the $a \times b$ plane in the crystal and exposed on the surfaces of the needle, which is in accordance with the preferred orientation on the (002) peak as observed in the XRD pattern. Figure 4(c) displays the SAED pattern recorded with the entire needle. The diffraction spots corresponding to (020), (321), and (301) planes indicate that the $Ce_{0.9}Sr_{1.1}Ga_3O_{7-\delta}$ needle is a single crystal with space group of $P\bar{4}2_1m$, $a \sim 8.04$ Å, and $c \sim 5.31$ Å. All these results confirm that the as-made $Ce_{0.9}Sr_{1.1}Ga_3O_{7-\delta}$ material in the present work has a needle-like morphology in nanoscale, which represents a rare example of material with nanoscale prepared by solid state reaction method, though the formation mechanism of these nanoscale needles remains unclear.

3.3. Thermal Redox Stability and Electrical Property. As the products of $Ce_{1-x}Sr_{1+x}Ga_3O_{7-\delta}$ are obtained under reducing atmosphere, their thermal redox stability in air was investigated from 50°C to elevated temperature at an interval of 50°C. Samples were annealed for 24 hours at each temperature and then cooled to room temperature, followed by XRD characterization and a typical phase evolution of the composition $Ce_{0.8}Sr_{1.2}Ga_3O_{7-\delta}$ was displayed in Figure 5(a). The results show that CeO_2 was detected in the products of $Ce_{1-x}Sr_{1+x}Ga_3O_{7-\delta}$ after being annealed at 650°C, which is similar to that of highly Ce-containing compositions in $La_{1-x}Ce_xSrGa_3O_{7+\delta}$ ($0.6 \leq x \leq 1$) as reported in our previous work [13].

Impedance measurements were carried out for $Ce_{1-x}Sr_{1+x}Ga_3O_{7-\delta}$ ceramic pellets in air below the decomposition temperature. Figures 5(a), 5(b), and 5(c) display the typical complex impedance plots recorded at 400°C of $Ce_{0.8}Sr_{1.2}Ga_3O_{7-\delta}$, $Ce_{0.9}Sr_{1.1}Ga_3O_{7-\delta}$ and $CeSrGa_3O_{7+\delta}$, respectively. All these plots comprise large and small semicircular arcs for grain and grain boundary responses, respectively. Usually, for a ceramic sample, the grain capacitance is in the order of ~10^{-12} F/cm and 10^{-11}–10^{-8} for grain boundary [17]. Here, take the sample $x = 0.2$; for instance, the capacitance values C calculated from the equation "$\omega_{max}RC = 1$" ($\omega_{max} = 2\pi f_{max}$, f_{max} is the frequency at the maximum of each semicircle) of the large and small arcs are 1.9×10^{-12} F/cm and 6.3×10^{-11} F/cm, respectively, which can be assigned to the grain and grain boundary response unambiguously. The grain boundary contributions of all these

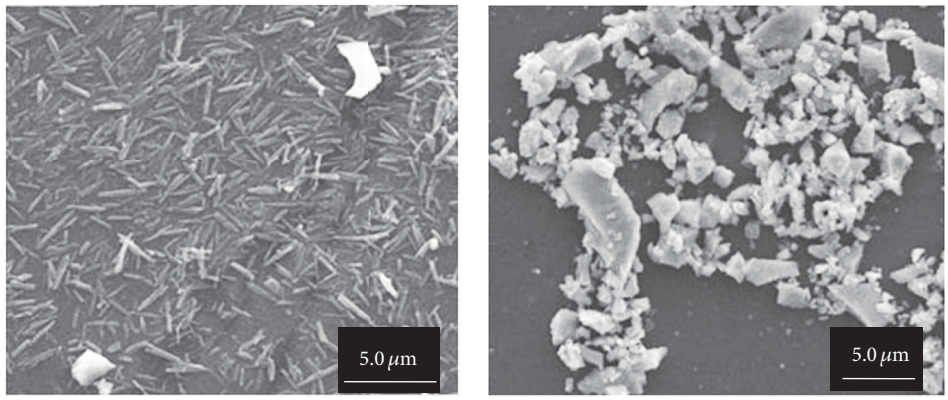

(a) (b)

Figure 3: SEM photos of $Ce_{0.9}Sr_{1.1}Ga_3O_{7-\delta}$ (a) and $CeSrGa_3O_{7+\delta}$ [14] (b).

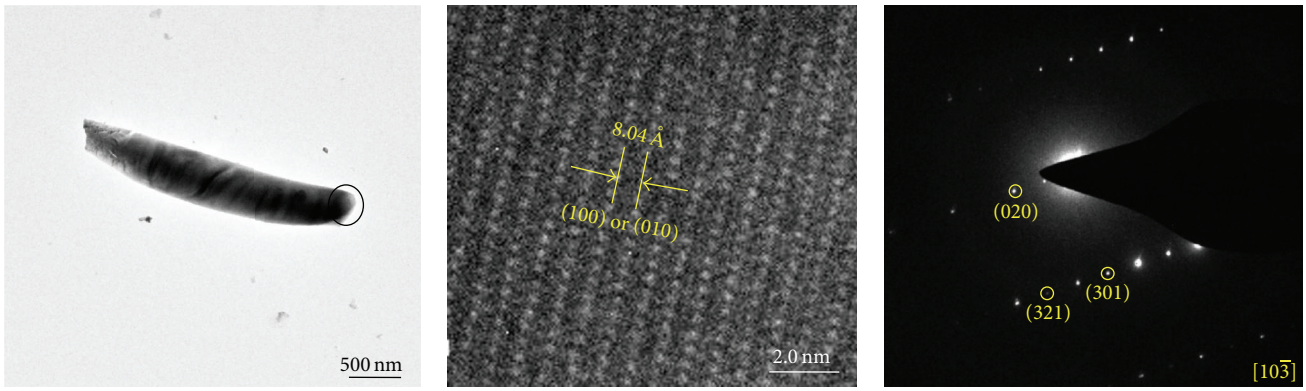

(a) (b) (c)

Figure 4: (a) TEM image. (b) HRTEM image record from the region marked by an open circle of the needle in (a). (c) SAED pictures of $Ce_{0.9}Sr_{1.1}Ga_3O_{7-\delta}$ material.

three samples are comparable to the bulk contribution, due to the low relative density of the ceramic pellets (60.8%, 59.4%, and 58.1% for $x = 0.2$, 0.1, and 0, resp.), similar to the Ce-rich compositions in $La_{1-x}Ce_xSrGa_3O_{7+\delta}$, as reported in our previous work [13]. A small tail with large capacitance of ~10^{-7} F/cm at low frequency was observed only for the $CeSrGa_3O_{7+\delta}$ material at 400°C, and this tail can be ascribed to the electrode response [17], which could be due to the mixed electronic and oxide ion conduction raised from the partial (~12%, as reported in our previous work [13]) oxidation of Ce^{3+} into Ce^{4+} in the as-made $CeSrGa_3O_{7+\delta}$ material. For $x = 0.1$ and 0.2, the oxidation states of Ce^{4+}/Ce^{3+} are more likely similar to those in the as-made $CeSrGa_3O_{7+\delta}$ due to the same preparing atmosphere. As revealed by the impedance plot, there is no ionic conduction in the composition $x = 0.1$ and 0.2, indicating the limited mobility of oxide vacancies in these materials. The Arrhenius plots for $Ce_{1-x}Sr_{1+x}Ga_3O_{7-\delta}$ together with those of $La_{0.2}Ce_{0.8}SrGa_3O_{7+\delta}$ which had been reported in our previous work [13] for comparison were given in Figure 5(d). As can be seen, the conductivity of $Ce_{1-x}Sr_{1+x}Ga_3O_{7-\delta}$ increases with the Ce content among the temperature range 300–600°C, which can be ascribed to the enhanced electronic conductivity arising from 4f electrons in Ce^{3+} cations [13]. However, although the Ce contents in $Ce_{0.8}Sr_{1.2}Ga_3O_{7-\delta}$ and $La_{0.2}Ce_{0.8}SrGa_3O_{7+\delta}$ are equal, the conductivity of $Ce_{0.8}Sr_{1.2}Ga_3O_{7-\delta}$ is higher than that of the latter. This may be explained by the fact that when part of of Sr^{2+} is replaced by smaller La^{3+} (1.16 Å in 8-coordinate cations) in the $Ce_{0.8}Sr_{1.2}Ga_3O_{7-\delta}$ material, resulting in a composition such as $La_{0.2}Ce_{0.8}SrGa_3O_{7+\delta}$ here, the contraction on the A-cationic size would increase, as it had been discussed in our previous work [13], which then aggravates the localization of charge carrier and thus resulting in a lower conductivity. As stated above, sample $x = 0.1$ shows a preferred orientation which usually would display particularity in some certain properties. Here, in this work, there seems no apparent correlation between the preferred orientation and conductivity property. As reported in the recently published work by Wei et al. [18], the melilite single crystal, taking the sample $La_{1.5}Ca_{0.5}Ga_3O_{7.25}$, for instance, has shown a strong anisotropic conduction. The ionic conductivity perpendicular to the c axis is ~0.036 Scm^{-1}, but only 0.8×10^{-2} Scm^{-1} along the c direction, indicating the preferred

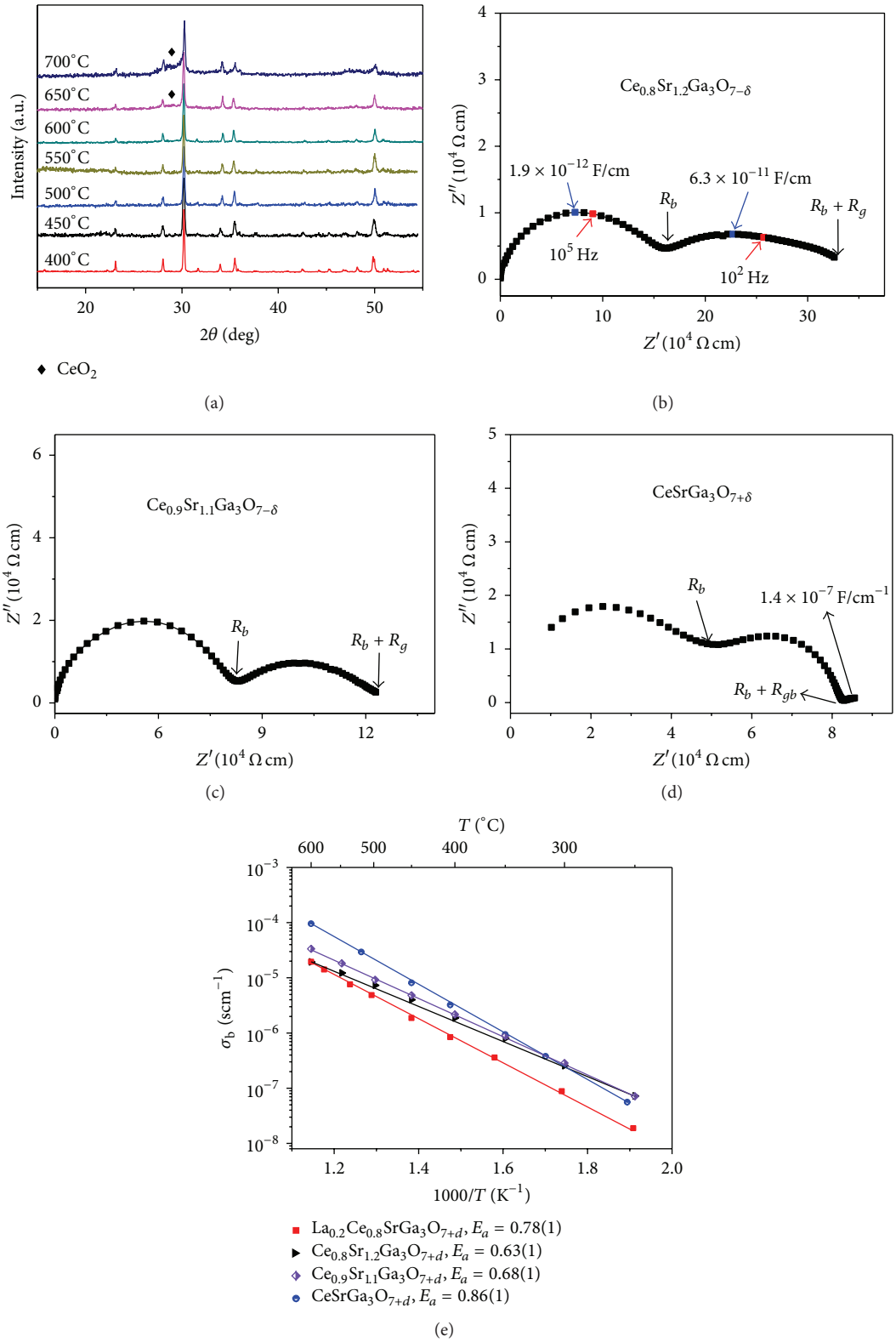

FIGURE 5: (a) Selected XRD patterns of $Ce_{0.8}Sr_{1.2}Ga_3O_{7-\delta}$ annealed at different temperature in air. (b, c, and d) Complex impedance plots of $Ce_{1-x}Sr_{1+x}Ga_3O_{7-\delta}$ recorded at 400°C. (e) Bulk conductivity of $Ce_{1-x}Sr_{1+x}Ga_3O_{7-\delta}$ together with that of $La_{0.2}Ce_{0.8}SrGa_3O_{7+\delta}$ [13] for comparison.

oxide ion diffusion pathway in the GaO_4 tetrahedral layer. In this paper, though a preferred orientation of grain growth was observed for $Ce_{0.9}Sr_{1.1}Ga_3O_{7-\delta}$, there is no apparent anisotropic conduction, which may be due to the polycrystalline nature of the measured ceramic pellet.

4. Conclusions

Materials $Ce_{1-x}Sr_{1+x}Ga_3O_{7-\delta}$ ($x \leq 0.3$) were synthesized by a solid state reaction method in CO-reducing atmosphere. For $x > 0.2$, single phase can not be obtained and typically $SrGa_2O_4$ and CeO_2 were presetted as impurity phases. Material $Ce_{0.9}Sr_{1.1}Ga_3O_{7-\delta}$ displays a uniform nanoscale needle-like morphology. These needles grow along a direction parallel to the *ab* plane and have an average length of ~2.5 μm and a diameter of ~500 nm. This provides a rare example of nanoscale materials prepared by solid state reaction method. The conductivity of $Ce_{1-x}Sr_{1+x}Ga_3O_{7-\delta}$ ($x \leq 0.2$) increases with the Ce content in the materials, due to the enhanced electronic conduction stemming from 4f electrons in Ce^{3+} cations.

Conflict of Interests

The authors declare that there is no conflict of interests regarding the publication of this paper.

Acknowledgments

This work is funded by Natural Science Foundation of Guangxi (no. 2015GXNSFBA139233), National Science Foundation of China (no. 21101174), and the Guangdong Province Research Project for industrial applications (nos. 2012B09000026 and 2011A090200083). The authors acknowledge the assistance from C. L. Liang for helping in the TEM, HRTEM, and SAED measurements.

References

[1] M. Kishimoto, H. Iwai, K. Miyawaki, M. Saito, and H. Yoshida, "Improvement of the sub-grid-scale model designed for 3D numerical simulation of solid oxide fuel cell electrodes using an adaptive power index," *Journal of Power Sources*, vol. 223, pp. 268–276, 2013.

[2] X. Kuang, J. L. Payne, M. R. Johnson, and I. E. Radosavljevic, "Remarkably high oxide ion conductivity at low temperature in an ordered fluorite-type superstructure," *Angewandte Chemie—International Edition*, vol. 51, no. 3, pp. 690–694, 2012.

[3] B. C. H. Steele and A. Heinzel, "Materials for fuel-cell technologies," *Nature*, vol. 414, no. 6861, pp. 345–352, 2001.

[4] A. Lashtabeg and S. J. Skinner, "Solid oxide fuel cells—a challenge for materials chemists?" *Journal of Materials Chemistry*, vol. 16, no. 31, pp. 3161–3170, 2006.

[5] D. J. L. Brett, A. Atkinson, N. P. Brandon, and S. J. Skinner, "Intermediate temperature solid oxide fuel cells," *Chemical Society Reviews*, vol. 37, no. 8, pp. 1568–1578, 2008.

[6] B. Liu, W. Guo, F. Chen, and C. Xia, "Ga site doping and concentration variation effects on the conductivities of melilite-type lanthanum strontium gallate electrolytes," *International Journal of Hydrogen Energy*, vol. 37, no. 1, pp. 961–966, 2012.

[7] C. Tealdi, P. Mustarelli, and M. S. Islam, "Layered $LaSrGa_3O_7$-based oxide-ion conductors: cooperative transport mechanisms and flexible structures," *Advanced Functional Materials*, vol. 20, no. 22, pp. 3874–3880, 2010.

[8] M. Rozumek, P. Majewski, L. Sauter, and F. Aldinger, "$La_{1+x}Sr_{1-x}Ga_3O_{7-\delta}$ melilite-type ceramics—preparation, composition, and structure," *Journal of the American Ceramic Society*, vol. 87, no. 4, pp. 662–669, 2004.

[9] X. Kuang, M. A. Green, H. Niu et al., "Interstitial oxide ion conductivity in the layered tetrahedral network melilite structure," *Nature Materials*, vol. 7, no. 6, pp. 498–504, 2008.

[10] A. J. Jacobson, "Materials for solid oxide fuel cells," *Chemistry of Materials*, vol. 22, no. 3, pp. 660–674, 2010.

[11] C. I. Thomas, X. Kuang, Z. Deng, H. Niu, J. B. Claridge, and M. J. Rosseinsky, "Phase stability control of interstitial oxide ion conductivity in the $La_{1+x}Sr_{1-x}Ga_3O_{7+x/2}$ melilite family," *Chemistry of Materials*, vol. 22, no. 8, pp. 2510–2516, 2010.

[12] M. Steins, W. Schmitz, R. Uecker, and J. Doerschel, "Crystal structure of strontium lanthanum trigallium heptoxide, $(Sr_{0.5}La_{0.5})_2Ga_3O_7$," *Zeitschrift für Kristallographie*, vol. 212, no. 1, p. 76, 1997.

[13] J. Xu, X. Kuang, E. Véron et al., "Localization of oxygen interstitials in $CeSrGa_3O_{7+\delta}$ melilite," *Inorganic Chemistry*, vol. 53, no. 21, pp. 11589–11597, 2014.

[14] A. Coelho, *TOPAS-Academic, Version 4.1*, Coelho Software, Brisbane, Australia, 2007.

[15] J. Xu, X. Li, F. Lu, H. Fu, C. M. Brown, and X. Kuang, "Oxygen interstitials and vacancies in $LaSrGa_3O_7$-based melilites," *Journal of Solid State Chemistry*, vol. 230, pp. 309–317, 2015.

[16] R. T. Shannon, "Revised effective ionic radii and systematic studies of interatomic distances in halides and chalcogenides," *Acta Crystallographica A: Crystal Physics, Diffraction, Theoretical and General Crystallography*, vol. 32, no. 5, pp. 751–767, 1976.

[17] J. T. S. Irvine, D. C. Sinclair, and A. R. West, "Electroceramics: characterization by impedance spectroscopy," *Advanced Materials*, vol. 2, no. 3, pp. 132–138, 1990.

[18] F. Wei, H. Gasparyan, P. J. Keenan et al., "Anisotropic oxide ion conduction in melilite intermediate temperature electrolytes," *Journal of Materials Chemistry A*, vol. 3, no. 6, pp. 3091–3096, 2015.

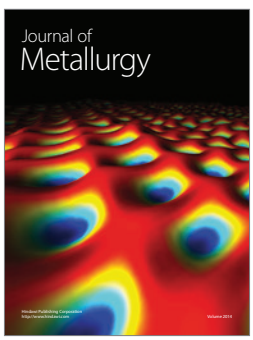

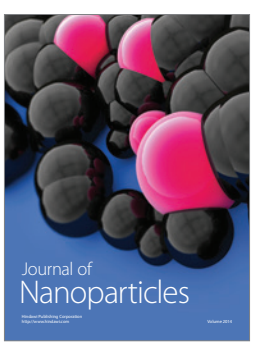

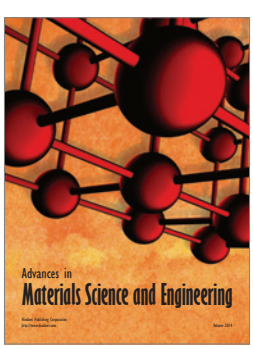

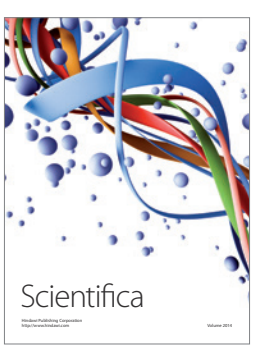

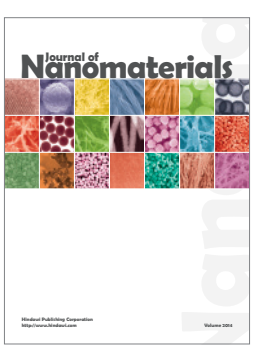

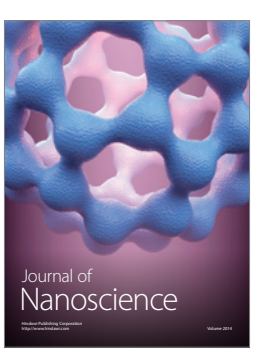

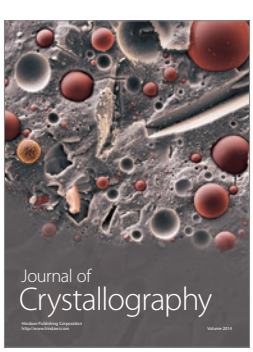

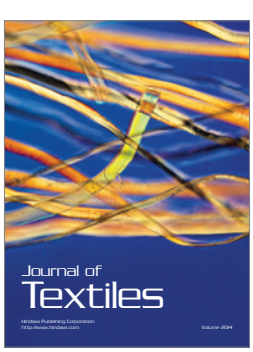

Hindawi

Submit your manuscripts at
http://www.hindawi.com